المجلة العراقية للبحوث الإنسانية والإجتماعية والعلمية
Iraqi Journal of Humanitarian, Social and Scientific Research
Print ISSN 2710-0952 Electronic ISSN 2790-1254
العدد 15A تشرين2 2024
No.15A Nov 2024

Inulin magnetized with Fe3O4 as a bionano adsorbent to clean contaminated water with crystal and methyl orange violet tinted

Selwan Mahdi Wanas Bada al-Ma'amouri
Salwanmahdy81@gmail.com

Abstract

Daar word tans gefokus op die ontwikkeling van 'n nuwe bio nano adsorbent van Fe3O4@inulin nanocomposite. Hierdie doelwit word bereik deur 'n in situ co-precipitation prosedure wat gebruik word om methyl orange (MO) en crystal violet (CV) dyes uit aqueous solutions te adsorb. Different physical characterization analyses confirmed the magnetic nanocomposite fabrication was successful. 'n Verskeidenheid van die aanvanklike dye konsentrasies, die dosering van die adsorbent, die pH en die temperatuur was gebruik om die adsorbent se vermoë om dye te verwyder te assesseer. Die konsentrasies was 5110 mg/L, 0.10.8 g/L, 111 en 283–338 K, respectively. As gevolg van die pH van zero point of charge en die intrinsieke eienskappe van die dyes, was die ideale pHs 5 en 7 vir MO- en CV-adsorption, respectively. In order to choose the best isotherm and kinetics models, the criteria used were the correlation of coefficient (R2) and the reduced chi squared value. Maximum adsorption capacity of 276.26 mg/g for MO and 223.57 mg/g for CV at 338 K was shown by the Langmuir model to be more appropriate for the adsorption data for beide dyes. Asook, in vergelyking met the pseudo first order and Elovich models, the pseudo second order model was more fit for kinetics data. Die endothermic and spontaneous nature of the dye adsorption process was demonstrated by the thermodynamic parameters. The increase in temperature supported the higher adsorption rate. Furthermore, after six consecutive cycles, the nanocomposite demonstrated exceptional capacity and stability, retaining over 87% of its initial dye removal efficiency. Overall, magnetized inulin with Fe3O4 can be an effective adsorbent to get rid of both anionic and cationic dyes from water.

Keywords: Magnetic inulin, Fe3O4, Crystal contaminated water cleaning, Colored methyl

الإينولين الممغنط مع Fe3O4 كمادة ماصة بيولوجية لتنظيف المياه الملوثة بالكريستال وبرتقالي الميثيل الملون البنفسجي

سلوان مهدي وناس بدع

الملخص

هناك كلمة واحدة تركز على تحسين مادة الامتصاص الحيوية النانوية الجديدة من Fe3O4inulin nanocomposite. يتم استخدام هذه الكلمة في عملية الترسيب المشترك في الموقع والتي تستخدم عبارة عن برتقال الميثيل (MO) والأصباغ البنفسجية الكريستالية (CV) من المحاليل المائية التي يتم امتصاصها.

أكدت تحليلات التوصيف الفيزيائي المختلفة أن تصنيع المركب النانوي المغناطيسي كان ناجحًا. في حالة تركيزات الصبغة اللاهوائية، يتم تقييم درجة الحموضة ودرجة الحرارة من خلال تركيز الصبغة. كانت التماثلات 5110 مجم/لتر، 0.10.8 جم/لتر، 111 و283–338 كلفن، على التوالي. كما هو الحال مع الرقم الهيدروجيني لنقطة الشحن الصفرية كانت الأصباغ الجوهرية هي درجة الحموضة المثالية 5 و 7 فير مو وامتصاص السيرة الذاتية، على التوالي. من أجل اختيار أفضل نماذج الأيسوثرم والحركية، كانت المعايير المستخدمة هي ارتباط المعامل (R2) وقيمة مربع كاي المخفضة. تم توضيح قدرة الامتزاز القصوى البالغة 276.26 مجم / جم لـ MO و 223.57 مجم / جم للسيرة الذاتية عند 338 كلفن بواسطة نموذج Langmuir لتكون أكثر ملاءمة لبيانات الامتزاز لأصباغ beide. Asook، في Vergelyking التقى بنماذج الدرجة الأولى الزائفة ونماذج Elovich، كان نموذج الدرجة الثانية الزائفة أكثر ملاءمة للبيانات الحركية. تم إثبات الطبيعة الماصة للحرارة والعفوية لعملية امتصاص الصبغة من خلال المعلمات الديناميكية الحرارية. الزيادة في درجة الحرارة دعمت ارتفاع معدل الامتزاز. علاوة على ذلك، بعد ست دورات متتالية، أظهر المركب النانوي قدرة وثباتًا استثنائيين، محتفظًا بأكثر من 87% من كفاءته الأولية في إزالة الصبغة. بشكل عام، يمكن أن يكون الأنسولين الممغنط مع Fe3O4 مادة ماصة فعالة للتخلص من الأصباغ الأنيونية والكاتيونية من الماء.

كلمات مفتاحية : الإينولين الممغنط ، Fe3O4 ، لتنظيف المياه الملوثة بالكريستال ، الميثيل الملون

Introduction

Rapid industrialization en die toename in menslike aktiwiteite het gelei tot ernstige omgewingskwessies regoor die wêreld, veral waterpollution. Daar is 'n algemene tendens dat 'n verskeidenheid organiese en inorganiese kontaminante daagliks in waterbronne van verskillende industrieë beland [1,2]. In die algemeen, die produksie van textile, plastic, cosmetica en papier bedryf produseer voortdurend skadelike dyestowwe in surface waters, wat skade aan mense, animals en die omgewing veroorsaak [3]. Daar is 'n groot aantal kommersiële dye beskikbaar regoor die wêreld, met meer as 10,000 spesimens beskikbaar, wat ongeveer 7 × 105 metric tons van dyes per jaar produseer[4]. Minder as 12% van dyes is wastes from manufacturing and handling processes, en 20% van die pollution by dyes is verantwoordelik vir industrial wastewater. Die feit dat baie dye-effluente sonder behandeling na nabygeleë waterbronne afgelewer word, is 'n groot bekommernis op die oomblik [5]. As gevolg van die feit dat hierdie dyes die deurdringing van sonlig deur die water verminder, is die aanwesigheid van hierdie dyes in water skadelik omdat dit die proses van aquatic plants se photosynthesis verminder. Furthermore, as gevolg van die presence of a number of poisonous substances, including chloride, aromatics, and heavy metals, these dyes can harm living beings[6]. Tot op 'n enkele spoor

quantity, water-containing dyes can cause cancer, skin issues, and allergic dermatitis [7]. Methyl orange (MO) is 'n algemene water-soluble, azo-anionic, organic synthetic dye wat uiters skadelik is vir beide organismes en die omgewing.

Crystal violet (CV), 'n triphenylmethane cationic dye, is ook uiters giftig. As gevolg van sy kragtige clastogenic eienskappe, kan dit in water ernstige gesondheids- en omgewingsprobleme veroorsaak. As gevolg hiervan moet alle water wat met hierdie kleurstowwe besmet word, onmiddellik regoor die wêreld behandel word. However, as a result of their non-biodegradability, thermal and photostability, the process is challenging and challenging [8,9]. Chemical, biological, and physical treatment methods including membrane filtration[10], coagulation[11], and electrodialysis have been used to treat dyes containing wastewater. en oksidasie van chemie[15]. Due to its superior characteristics, adsorption has received a lot of attention among them. In vergelyking met ander metodes, adsorption het baie voordele; dit is maklik om te gebruik, koste-effektief, het 'n lae operasietemperatuur, geen secondary pollution, is eenvoudig, en elimineer pollutants direk uit die stelsel[16]. So far, 'n verskeidenheid adsorbents, soos carbonaceous materials, have been gebruik om dit te bereik. As gevolg van hul hoë regeneration koste, lae sorption efficiency, en ingewikkelde separation proses, word hulle tipies nie gebruik om dye-polluted water te behandel nie[17]. In die afgelope drie jaar het'n aantal wetenskaplikes probeer om omgewingsvriendelike, chitosan-gebaseerde bio-nanocomposites wat magnetiseer met metal oxides te skep as adsorbente vir die behandeling van water en wastewater [18]. Jawad en kollegas: [19] gemaak van 'n nuwe hybrid bio-adsorbent wat 'n cross-linked chitosan-epichlorohydrin/TiO2 nanocomposite is. Dit het 'n maksimum adsorption capacity van 210 mg/g at 30 °C. They discovered that three factors were responsible for the adsorption of dye molecules on the adsorbent surface: electrostatic attraction, H-bonding, and n-π stacking. Reghioua en kollegasIn 'n poging om Remazol se briljante blou R-kleurstof uit wastewater te verwyder, is 'n Schiff-basiese chitosan-glutaraldehyde composite geskep wat magnetiseer is deur Fe3O4 en ZnO. By adding 25% ZnO to the nanocomposite structure, was the high est capacity found to be 176.6 mg/g at 60 °C. Kazemi and Javanbakht [21] created a magnetic zeolite/chitosan/alginate nanocomposite that was stable by crosslinking it with CaCl2 and glutaraldehyde.. The findings showed that the synthetic adsorbent adsorbs metylene blue spontaneously. Al-Musawi et al. [22] gebruik magnetite Fe2O3 nanoparticles om 'n chitosan polymer te bedek, wat gelei het tot die adsorption van acid blue 113 dye uit 'n aqueous solution. Die eksperimentele faktore wat ondersoek is, sluit in die eerste dye konsentrasie, die pH van die solution, die dosage van die nanocomposite, die tyd wat die adsorption plaasvind, en die temperatuur. In the best conditions, they found a maximum uptake capacity of 128 mg/g and a dye removal efficiency of 99.63%, respectively. Tanhaei et al. [23] het 'n chitosan-gebaseerde adsorbent magnetized with carbon-Fe3O4 core-shell nanoparticles ontwikkel om methyl orange uit aqueous solutions te verwyder. Hierdie adsorbent het 'n maksimum uptake capacity van 425 mg/g at

45 °C. Neves en kollegas24) magnetized chitosan with a newly developed graphene oxide derivative and added arenediazonium salts to enhance its amphiphilic properties and broaden its adsorption spectrum. A maximum dye removal capacity and rate of 650 mg/g and 95% was both achieved by the magnetized sorbent. In die proses om basic brown 4 uit aqueous solutions te verwyder, demonstreer hul magnetic composite die vermoë om as 'n filtering agent te funksioneer deur die eenvoudige verwijdering daarvan deur die magnetiese veld. Hernández-Martínez et al.[25] gesê inulin kan chitosan vervang, veral vir die verwydering van Pb2+ uit wastewater., to increase the scalability and production cost of producing polyurethane-based nanocomposites. Inulin is a member of the fructan group of polysaccharides and is composed of linear fructose polymers with different chain lengths as well as a glucose molecule at every C2 end [26]. As a substance that is generally classified as safe (GRAS), A host of microorganisms, which is widely found in nature as a storage carb, can produce inulin. Chicory word vir kommersiële doeleindes gebruik om inulin te produseer, wat deels in water opgelos is, wat dit moontlik maak om by aqueous media by te voeg sonder om enige precipitasie te veroorsaak [27]. Chicory inulin production process is shown in Supplementary Figure S1.. In order to first remove anionic and cationic dyes from water, this study aims to fabricate a new biocompatible adsorbent of Fe3O4@inulin nanocomposite. 'n Verskeidenheid analyses, soos scanning electron microscopy (SEM) with energy dispersive X-ray analysis (EDX), X-ray powder diffraction (XRD), thermogravimetric analysis (TGA), Brunauer–Emmett–Teller (BET), and vibrating sample magnetometry (VSM), het die prepared adsorbent geïdentifiseer. Kinematiese en isotermiese studies het ook die adsorption van MO en CV dyes met die synthesized adsorbent ondersoek. Last but not least, the adsorbent reusability was assessed following a number of reusing cycles.

Materials and methods

Materiaal Iron (II) chloride tetrahydrate (FeCl2 - 4H2O (aq)), iron (III) chloride hexahydrate (FeCl3 - 6H2O (aq), ammonia (NH3, 25%), hydrochloric acid (HCl - 0.1 M), sodium hydroxide (NaOH - 0.1 M), chicory inulin, methyl orange and crystal violet dyes was alles gekoop by Sigma-Aldrich. All materials were used in their analytical grades unfiltered. Fig. 1a and Fig. 1b show the molecular structures of crystal violet and methyl orange as dye contaminants.

Die vorming van Fe3O4@inulin. First, a 250 mL two-mouth glass f lask was filled with 60 mL of deionized water. 0.7 g van FeCl2·4H2O is opgelos. into the flask while stirring. Then, 1.9 grams of FeCl3·6H2O was added to the solution. To get a even solution, stirred the mixture for five minutes until it completely dissolved. Next, 0.75 g of inulin was slowly added to the solution in multiple stages while

stirring for 25 minutes. Under a nitrogen atmosphere was die atmosfeer se temperatuur verhoog tot 85 °C, en 10 mL of NH3OH was dropwise ingespuit vir 70 minute. The solution became black, which indicates the creation of Fe3O4 nanoparticles during the injection. For thirty minutes, the mixture was stirred again to allow the remaining NH3OH to react. Next, a magnet was used to separate the magnetized inulin nanoparticles from the solution and wash them.

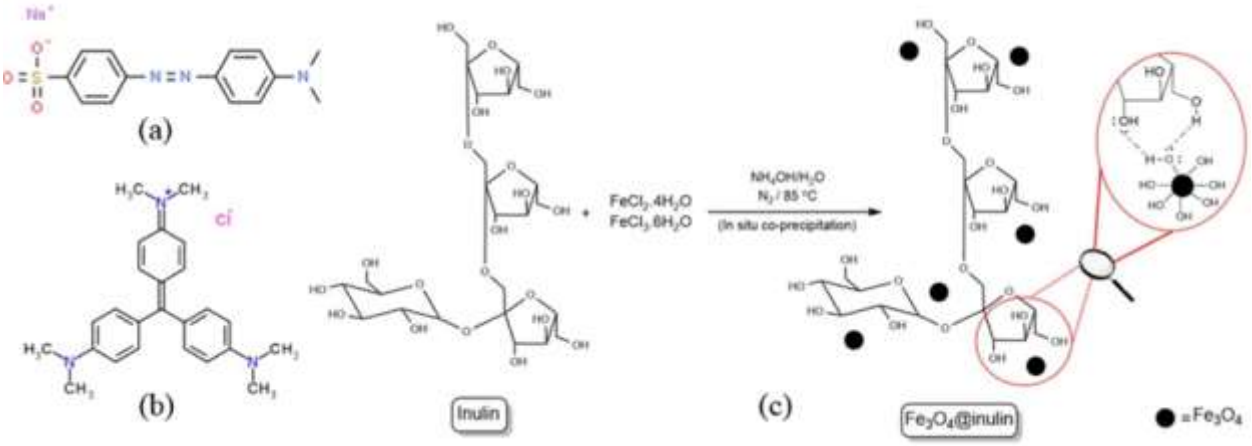

Figure 1. Molecular structures of (a) methyl orange, (b) crystal violet, and (c) Fe3O4@inulin with synthesis procedure.

with four times deionized water to get rid of unreacted materials from the nanocomposite. The magnetized inulin was moved to an oven and was dry for 15 hours at 55 °C. Last but not least, the powdered nanoparticles were acquired for the experiments and characterization. The molecular scheme of the Fe3O4@inlulin synthesis process is shown in Figure 1c.

Characterization.

An XRD analysis (STOE STADI-MP model, Germany) was used to investigate the crystal network of the synthesized adsorbent nanoparticles. Cu Ka radiation (= 1.54 Å) and 2θ was measured from 10° to 80°. FTIR-analise is gebruik om die funksionele groepe van adsorbente te assesseer (Spectrum Rx1 model, Perkin Elmer Co.).) tussen 400 en 4000 cm1. A VSM device (LBKFB model, Iran) was used to evaluate the magnetization properties of the prepared nanocomposite under the ambient conditions and in a range from 4000 to 4000 Oe. By means of SEM–EDX analysis (MIRA3 TESCAN), the adsorbent's structure, morphology, and

elemental distribution were determined. By verwarming BET-analise is uitgevoer op 77 K op die monster at 120 °C om enige strukturele impurities te verwyder (Micromeritics, Model ASAP 2020, USA). In order to determine the point of zero charges (PZC), several 0.1 M NaNO3 solutions was added to several flasks at the ambient condition. By using a pH meter, the initial pH values (pHi) were adjusted by adding solutions of HCl and NaOH. 'n Sample van 2 gram is by elke mengsel gevoeg en dan vir 48 uur onder omgewingstoestande gemeng. In order to determine the pH of zero point of charge (pHZPC), kan die final pH values (pHf) bepaal word.

Adsorption experiments.

In order to assess the adsorption capabilities of synthesized magnetic nanocomposites, the following experiments with dye removal were conducted. Batch adsorption was uitgevoer in 'n Erlenmeyer flask met 'n volume van 250 mL deur 0,1–0,8 g van die magnetic bio-nano adsorbent by te voeg in controlled operational conditions for isotherm and kinetics studies. The initial concentration (Cdye) of MO and CV was between 25 and 200 mg/L. Every solution had a volume of 100 milliliter, en the adsorption temperature was between 10 en 65 grade Celsius. In order to determine the optimal conditions for each dye removal, the solution pH was taken into account in a range from 1 to 11. To achieve this, the calibration curves for both dyes were first plotted. at verskillende pH's. Daarbenewens is eksperimente met adsorption uitgevoer met verskillende pH's en verskillende tydperke van adsorption (15 tot 180 minute, met sampling elke vyftien minute). Finally, to determine the concentration of the remaining dye in the aqueous solution, was a calibration curve whose pH was proportional to the corresponding solution pH. Daar is gebruik gemaak van 'n UV–Vis spectrophotometer (Rayleigh/UV 2601) met 'n wavelength van 464 nm vir MO en 590 nm vir CV om die konsentrasies van die dye te bepaal. Following is the formulas for removal efficiency (Q) and adsorption capacity(28).

$$\text{Removal } (\%) = \frac{C_0 - C_e}{C_0} \times 100 \qquad (1)$$

$$Q \text{ (mg/g)} = \frac{(C_0 - C_e)V}{m} \qquad (2)$$

in which the initial and equilibrium concentrations of dyes in the aqueous solution are C0 and Ce (mg/L). Die massa van die nanocomposite is m (g) en die volume

van die aqueous solution is V (L). Every experimental run was repeated three times, and all the results were reported as averaged data with a deviation error of plus or minus 5%.

Results and discussion

Adsorbent characterization.

FTIR analysis is a practical tool for detecting the functional groups in the structure of materials. Figure 2a presents the FTIR spectra of Fe3O4, inulin, and Fe3O4@inulin compounds. In the Fe3O4 spectrum, there is a prominent peak related to the FeO bond at 578 cm−129. The FTIR spectra of inulin

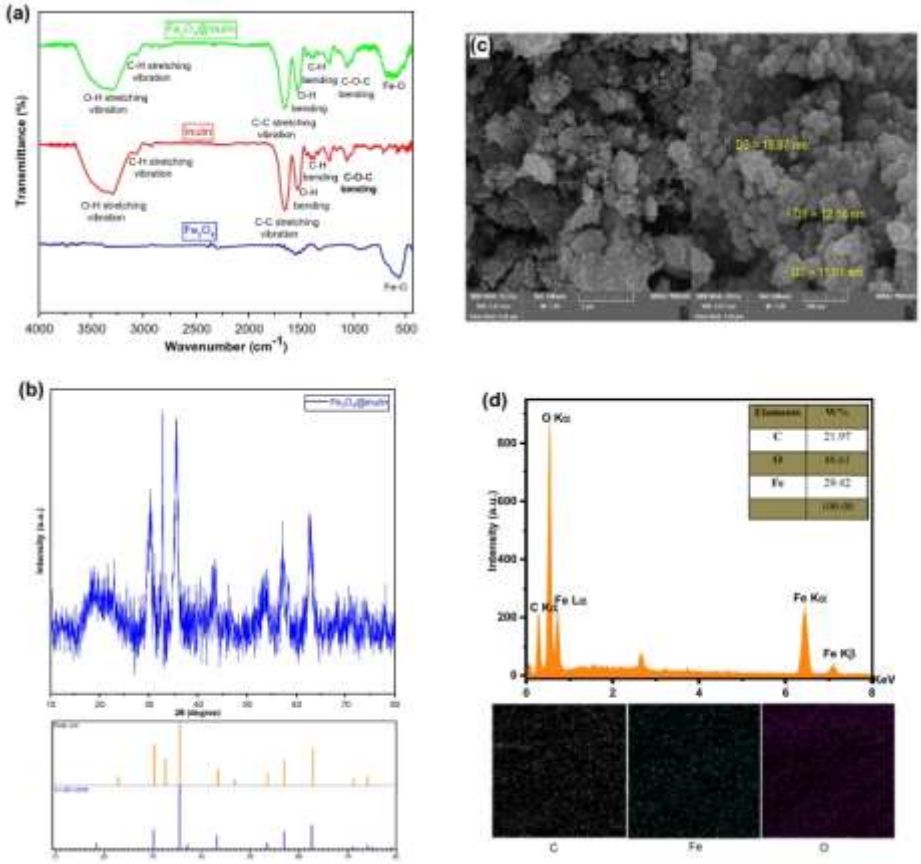

Figure 2. (a) FTIR spectra of Fe3O4, inulin, and Fe3O4@inulin; (b) XRD pattern of the prepared Fe3O4@inulin nanocomposite; (c) SEM images and (d) EDX results of the synthesized Fe3O4@inulin bio-nano adsorbent

Daarbenewens toon Fe3O4@inulin nanocomposite baie soortgelyke adsorption bands. Die breë adsorption bands van 3428 cm1 en 1531 cm1 word geassosieer met die bending en stretching vibrations van die OH-bond [30], wat baie voorkom in die inulin backbone. The CH bond's stretching vibration is linked to the adsorption band at approximately 3095 cm1. The COC bond's asymmetric stretching vibration has a peak at 1101 cm1, and the COC bond's absorption band has a peak at 1052 cm1. In addition, the presence of the FeO peak in the Fe3O4@inulin spectrum indicates the successful manufacture of the nanocom posite. Die kristalstruktuur van Fe3O4@inulin nanocomposite is ondersoek deur XRD-analise. is shown in Fig. 2b. The amorphous phase of inulin is indicated by an individual weak broad peak between 15° and 23°. According to the Fe3O4 standard patterns in card no. JCPDS, 01-087-0246, this magnetic substance has some broad characteristic diffraction peaks at 2θ of 18.27°, 30.07°, 35.46°, 37.13°, 43.02°, 57.16°, 62.74°, 71.21°, and 73.49°32. Die skerp en wye peaks wys die kristalline en amorphous areas van die Fe3O4@inulin nanocomposite. Die gemiddelde kristalgrootte van Fe3O4@inulin bio-nano adsorbent is 10.9 nm, volgens Scherer se equation33. As a way to assess the morphology and elemental distribution of the Fe3O4@inulin adsorbent, SEM–EDX analysis has been performed, as presented. in Fig. 2c,d. As shown in Fig. 2c The surface morfology of Fe3O4@inulin nanocomposite is rough, heterogeneous, and irregular at low magnification, with some cavities. Nevertheless, the SEM images at higher magnifications show a relatively uniform, regular surface.

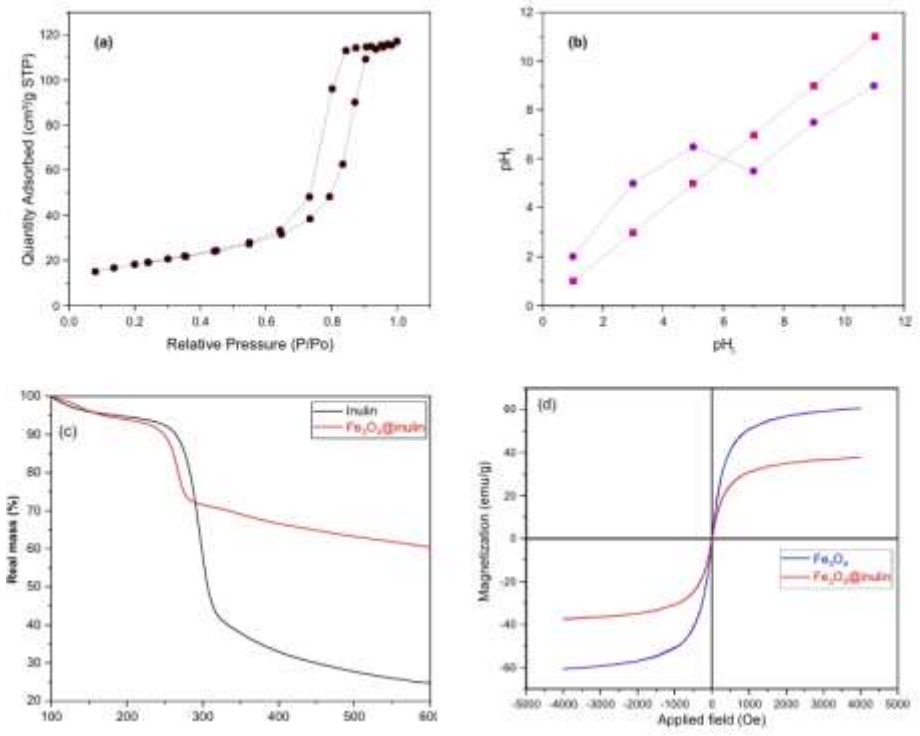

Figure 3. (a) N2 adsorption/desorption curve of the Fe3O4@inulin adsorbent; (b) pHf versus pHi for determining pHZPC of the Fe3O4@inulin nanocomposite; (c) TGA curves of inulin and Fe3O4@inulin; (d) magnetic hysteresis curves of Fe3O4 and Fe3O4@inulin

verspreiing van ronde nanoparticles op die Fe3O4@inulin nanocomposite surface, met diameters van 10–20 nm. Furthermore, the elemental mapping in Fig. 2d toon dat elke element—carbon, oxygen, and iron—aan 'n gelyke wyse in the adsorbent structure verdeel is. The oxygen content, with 48.61%, is the highest. Fig. 3a toon die N2 adsorption/desorption isotherm van die synthesized Fe3O4@inulin nanoparticles. Hierdie resultate van die BET-analise word getoon. The mesoporous structure of the adsorbent supported by the type IV isotherm based on the IUPAC classification34 is shown on this curve. Such mesopores help to enhance the material's specific surface area. [35], Fe3O4@inulin adsorbent has a specific surface area of 66.15 m2/g, a pore volume of 0.181 cm3/g, and an average pore diameter of 11.027 nm. The adsorbent surface charge is displayed by the factor pHPZC, which is the pH value at which the net surface charge is zero. For the prepared Fe3O4@inulin composite, pHf against pHi values are plotted in Fig. 3b. This factor shows a pHPZC of about 6. As gevolg hiervan sal die adsorbent se oppervlak positief gechargeer wees wanneer die pH hoër as 6. Die magnetic thermal resistance is gemeet deur die TGA-metode te gebruik. Fe3O4@inulin in temperature tussen 100 en 600 grade Celsius in die atmosfeer. The weight loss curve of both pure inulin and Fe3O4@inulin materials is shown in Figure 3c. As gevolg van free water and moisture evaporation in the elimi nation, both substances lost about 9% in weight. Inulin se grootste decomposition koers vind plaas tussen 240 en 310 °C, met 'n 50% vermindering in sy massa. Dit kan verband hou met dehydration. Nevertheless, the most significant weight loss of the Fe3O4@inulin nanocomposite occurs at 240–285 °C, with a decrease of about 20%, representing potensieel die primêre afbreek van die magnetic composite as gevolg van selective dehydration. Die oorblywende massas van inulin by 600 °C is ongeveer 25% en Fe3O4@inulin is ongeveer 65%. As gevolg hiervan, deur magnetic Fe3O4 nanoparticles in die inulin matrix in te sluit, is dit moontlik om die matrix se thermal stability aansienlik te verhoog as gevolg van die sterk intermolekulêre interactions wat dit het. VSM analysis is used to assess magnetized inulin's magnetic properties. The magnetic hysteresis loop of Fe3O4 and Fe3O4@ is shown in Figure 3d.

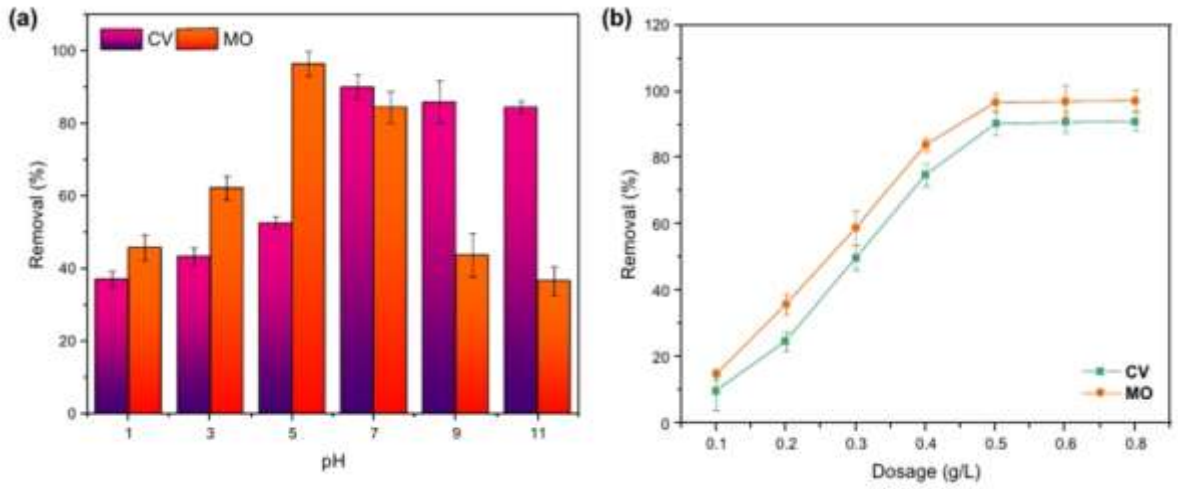

Figure 4. (a) Effect of solution pH (Ca = 0.5 g/L, Cdye = 25 mg/L); (b) Effect of adsorbent dosage (optimum pH = 7 for CV and 5 for MO) on the dye removal efficiency; T = 25 °C, t = 180 min

nanodeeltjies van inulin. Fe3O4@inulin nanocomposite has a magnetic saturation of 40.21 emu/g. wat 34% laer is as die Fe3O4 nanoparticles. The presence of non-magnetic inulin—inulin—in the structure of the synthesized composite is the cause of this lower saturation. Nevertheless, this minor reduction in magnetic saturation is reasonable, and by using an external magnetic field or a simple magnet, the nanocomposite can still be effectively taken out of the reaction solution.

Effect of operating conditions.

Experiments met adsorption is uitgevoer op verskeie pH's, rangskik van 1–11 to f, met die doel om die optimale pH te vind vir elke dye. Die ander operasiefaktore bly dieselfde: die temperatuur was 25 °C, die dosering van adsorbent was 0,5 g/L, die konsentrasie van dye was 25 mg/L, en die adsorptionstyd was 180 minute. As bekend, molecular aggregation occurs in aqueous solutions when the pH value is very low, resulting in con siderable aggregates. As gevolg hiervan is dit logies om die optimale pH vir elke solution te identifiseer. The dye removal efficiency is shown in Figure 4a at different solution pHs. Maximum adsorption rates van ongeveer 95% vir MO dyes en 91% vir CV dyes was gevind by 'n pH van 5. soortgelyke tendense in adsorption The pHZPC curve, shown in Figure 3b, can be used to explain the variation. The net surface of amphoteric molecules with positive and negative charges is affected by the solution pH. By wyse van 'n

toename of afname in protons, kan hulle meer positief of negatief gechargeer word. In highly acidic solutions fungeer MO as a cationic dye36. As gevolg hiervan is die removalsvermoë laer as gevolg van die electrostatic repulsion between die cationic dye en die negatively charged adsorbent surface. By increasing the solution pH further, the number of positive charges decreases. At pH 5, MO removal efficiency is optimal. However, at a pH higher than 5, its adsorption rate will be lower as a result of electrostatic repulsion and an excess of hydroxyl ions competing with MO molecules for adsorption sites. Verder is die kleur van shallow, as gevolg van beide die verandering in pH en die verband met die adsorption van Fe3O4@inulin adsorbent. Daar is 'n moontlikheid dat 'n oormaat H+ ions in aanraking kom met CV dye cations vir die adsorption sites, wat lei tot 'n laer removalskoers vir CV adsorption by 'n acidic pH37. The CV removal efficiency does not significantly change under a pH higher than the neutral solution. As gevolg hiervan is die optimale pH waarde vir CV removal gevind om 7 te wees. Figure 4b wys hoe die Fe3O4@inulin adsorbent dosage die removal efficiency van die twee dyes beïnvloed, met konsentrasies wat tussen 0.10.8 g/L en verder wissel. Die optimale pH-oplossing met betrekking tot elke In hierdie gevalstudie is die dye in ag geneem. When the adsorbent dosage is 0.1 g/L for MO adsorption and 9.1 g/L for CV adsorption, the removal efficiencies are about 6.3 times. Increased active binding sites and improved active functional groups in the nanocomposite are responsible for this significant increase. Because of the saturation of adsorption sites, removal efficiency does not significantly increase at dosages above 0.5 g/L. So, for the next tests, the best adsorbent to adsorb both dyes is 0.5 g/L.

Adsorption isotherms.

On the basis of adsorption isotherm models, it is possible to determine the relationship of equilibrium between the adsorbent and adsorbate. Four non-linear isotherm models—Langmuir, Freundlich, Dubinin–Radushkevich (D–R) and Temkin—was used to estimate the adsorption behavior of the prepared Nano composite. The correlations between hulle is given below. [38]:

$$\text{Langmuir:} \quad Q_e = \frac{Q_m K_L C_e}{1 + K_L C_e} \qquad (3)$$

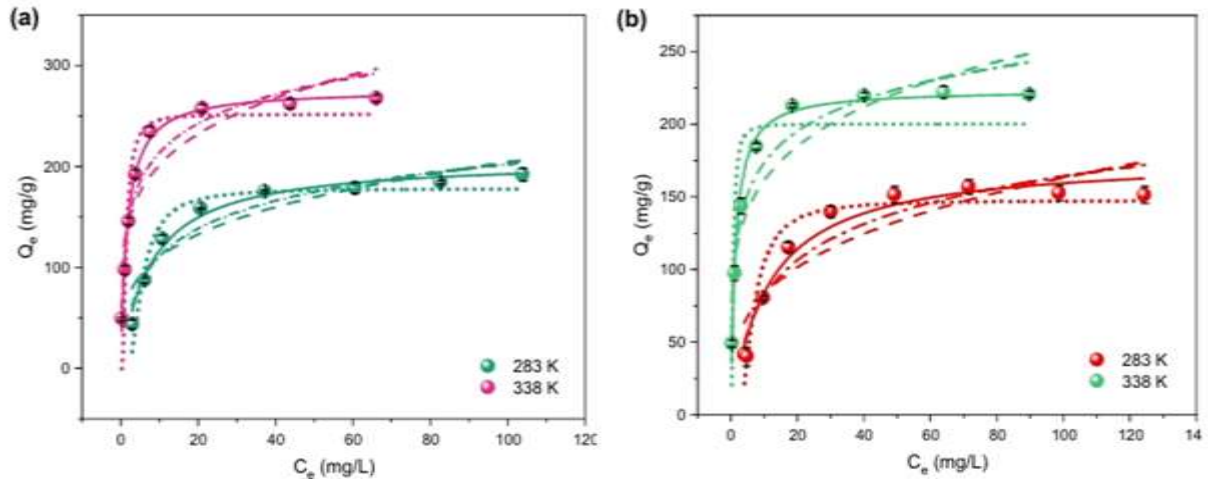

Figure 5. Isotherm curves under different temperatures for (a) MO adsorption at pH of 5 and (b) CV adsorption at pH of 7; solid lines: Langmuir, dashed lines: Freundlich, dotted lines: Dubinin-Radushkevich, dash-dotted lines: Temkin.

$$\text{Freundlich:} \quad Q_e = K_F C_e^{\frac{1}{n}} \tag{4}$$

$$\text{Dubinin-Radushkevich:} \quad Q_e = Q_m \exp\left(-K_D\left(RT\ln\left(1+\frac{1}{C_e}\right)\right)^2\right) \tag{5}$$

$$\text{Temkin:} \quad Q_e = \frac{RT}{B_T}\ln(K_T C_e) \tag{6}$$

Where Qe is the quantity of dye adsorbed at the equilibrium state, Qm is the Langmuir monolayer adsorption capacity, KL is the Langmuir isotherm constant, KF is the Freundlich isotherm constant, and n is the Freundlich exponent39. R is the gas constant (8.314 J/mol K), KD is the isotherm constant in the thermodynamic equilibrium constant in the adsorption process, and T is the temperature. In addition, KT and BT are referred to as the Temkin isotherm constant and a constant related to adsorption heat, respectively. When ideal monolayer adsorption occurs on a homogeneous surface, the Langmuir isotherm is usually used cally. Friendly isotherms are usually suitable for surfaces wat heterogene is. Volgens die Freundlich isotherm model, wat heeltemal empiries is, word veronderstel dat 'n groot aantal existing sites op dieselfde tyd aktiwiteit vertoon, elk met 'n verskillende soort free sorption energy. As gevolg van the D-R model, the adsorption potential, regardless of temperature, can represent the

adsorption equilibrium relation for a particular combination of adsorbents and adsorbates. Volgens die Temkin isotherm model verminder elke molecule se adsorption-hitte proporsioneel met die toename in die dekking van die adsorbent se surface, en adsorption word gekenmerk deur 'n uniforme verspreiding van binding energies. Fig. 5 toon isotherm modeling of MO and CV adsorption onto the Fe3O4@inulin composite at 283 K and 338 K, respectively. Die uitkomste en pas Table 1 verskaf parameters vir alle isothermmodelle vir temperature binne hierdie reeks. The dosage of the adsorbent in this study is 0.5 g/L, and the time of adsorption is 180 minute. Due to a coefficient of determination (R2) higher than 0.98 and the lowest reduced chi-squared value of any model studied, the Langmuir isotherm model showed a better prediction for the adsorption data related to both dyes at all temperatures. As die temperatuur styg, neem die nanocomposite se adsorption krag toe, wat beteken dat hoër temperature die MO- en CV-adsorption prosesse bevoordeel, aangesien die nanocomposite endothermies is. In addition, in the Freundlich isotherm model, the constant (KF) value is higher at high temperatures, which shows that adsorption This Dit is moontlik dat die toename in adsorption rate te wyte is aan die feit dat sekere interne bonds op die komposiete aktiewe oppervlak deur temperatuur vernietig word. Hierdie proses veroorsaak dat meer adsorption sites geskep word en dat dye molekules deur 'n temperatuurtrigger in composite surface cavities versprei word. Verder toon Freundlich-modelle waardes van 1/n wat minder as 1 is by alle temperature, wat 'n gunstige adsorptionsproses aandui.

Adsorption kinetics.

When dit kom by die adsorption van pollutants uit contaminated water, kan kinetics studies nuttig wees omdat dit ons in staat stel om die adsorption equilibrium time, adsorption kinetics rate, en die konsentrasie van die pollutant in elke stap nadat ons die equilibrium state bereik het. In hierdie geval word pseudo-first-order (PFO), pseudo-second-order (PSO), and Elovich kinetics models gebruik om die adsorption mechanism of MO and CV dyes onto the Fe3O4@inulin

nanocomposite beter te ondersoek.

Model	Dye	MO				CV			
	Temperature [K]	283	298	318	338	283	298	318	338
Langmuir	K_L [L/mg]	0.1289	0.2296	0.2869	0.6137	0.0902	0.1586	0.3079	0.7581
	Q_m [mg/g]	207.42	223.64	255.23	276.26	177.14	192.88	209.95	223.74
	Reduced chi-squared	59.749	49.023	36.121	52.880	83.947	46.669	17.638	85.860
	R^2	0.9819	0.9888	0.9941	0.9934	0.9683	0.9868	0.9962	0.9860
	Adjusted R^2	0.9789	0.9870	0.9931	0.9923	0.9638	0.9849	0.9957	0.9840
Freundlich	K_F [(mg/g)(L/mg)$^{1/n}$]	59.477	79.173	93.948	125.571	41.901	57.730	77.454	102.27
	n [dimensionless]	3.732	4.198	4.184	4.872	3.384	3.829	4.353	5.061
	Reduced chi-squared	471.78	414.04	764.35	1184.01	452.68	528.32	699.24	693.89
	R^2	0.8572	0.9069	0.8759	0.8523	0.8296	0.8508	0.8621	0.8869
	Adjusted R^2	0.8334	0.8902	0.8552	0.8277	0.8062	0.8296	0.8310	0.8708
Dubinin–Radushkevich	K_D	4.8122	2.1686	1.2620	3.1610	6.9059	2.0001	5.5347	1.0984
	Q_m	178.47	199.62	228.64	251.93	147.84	164.55	184.23	200.33
	Reduced chi-squared	233.84	666.68	605.74	730.41	186.25	418.77	516.45	966.34
	R^2	0.9292	0.8484	0.9016	0.9089	0.9298	0.8817	0.8907	0.8425
	Adjusted R^2	0.9174	0.8232	0.8852	0.8937	0.9198	0.8648	0.8751	0.8200
Temkin	B_T	59.182	66.753	61.144	67.504	66.476	70.141	75.979	88.877
	K_T	1.6319	4.8942	5.3783	16.962	0.9660	2.2236	5.5592	24.041
	Reduced chi-squared	218.68	138.69	289.24	492.37	220.70	235.52	297.04	229.57
	R^2	0.9338	0.9684	0.9530	0.9386	0.9169	0.9335	0.9371	0.9626
	Adjusted R^2	0.9227	0.9632	0.9452	0.9283	0.9050	0.9240	0.9281	0.9572

Table 1. Fitting parameters obtained from isotherm models for the MO and CV adsorption onto the Fe3O4@ inulin nanocomposite.

As gevolg van the PFO model, is the rate of variation in solute adsorption directly proportional to the variation in saturated concentration as well as the amount of adsorptive solid adsorbed over time. Volgens PSO-kinetics word die adsorption rate bepaal deur die interaction between the adsorbate and adsorbent species. The Elovich model can calculate the adsorption system's surface and mass diffusion, activation and deactivation energy. In hierdie model verhoog die hoeveelheid solute wat adsorbeer 'n eksponensiële afname in die solute adsorption rate41. These models' non-linear equations are as follows: [42]

$$\text{PFO:} \quad Q_t = Q_e(1 - \exp(-k_1 t)) \tag{7}$$

$$\text{PSO:} \quad Q_t = \frac{k_2 Q_e^2 t}{1 + Q_e k_2 t} \tag{8}$$

$$\text{Elovich:} \quad Q_t = \frac{1}{\beta} \ln(\alpha\beta t + 1) \tag{9}$$

where k1 and k2 are the rate constants for the PFO and PSO models, and Qt is the amount of dye adsorbed at time t. In addition, the initial adsorption rate and desorption constant in the Elovich model are the terms and. Fig. 6 toon die fitting resultate van kinetic data. The PSO model, one of these three models, provides excellent predictions for both dyes' experimental kinetics data regarding the adsorption capacity of the prepared nanocomposite. Die parameters wat geskep is deur die kineticsmodelle aan die eksperimentele data te pas, is in Table 2. The highest R2 and lowest reduced chi-squared values confirm that a PSO kinetics can describe the adsorption mechanism. die model. This model shows that both dyes are adsorbed onto the Fe3O4@inulin adsorbent surface via a chemisorption process43. In ander woorde, the mol ecules of the dyes are bound to the Fe3O4@inulin via surface exchange reactions. Fig. 6b shows the dye adsorption mechanism of the prepared Fe3O4@inulin nanocomposite. Electrostatic attraction and hydrogen bonding interactions are the most important forces (dipole–dipole and Yoshida). Each force's contribution to dye adsorption varies by different pHs, as can be seen in the literature. [44].

Thermodynamic study.

The following correlations were used to determine the thermodynamic parameters of the enthalpy (H°), entropy (S°), and Gibbs free energy (G°):

$$K_c = \frac{Q_e}{C_e} \tag{10}$$

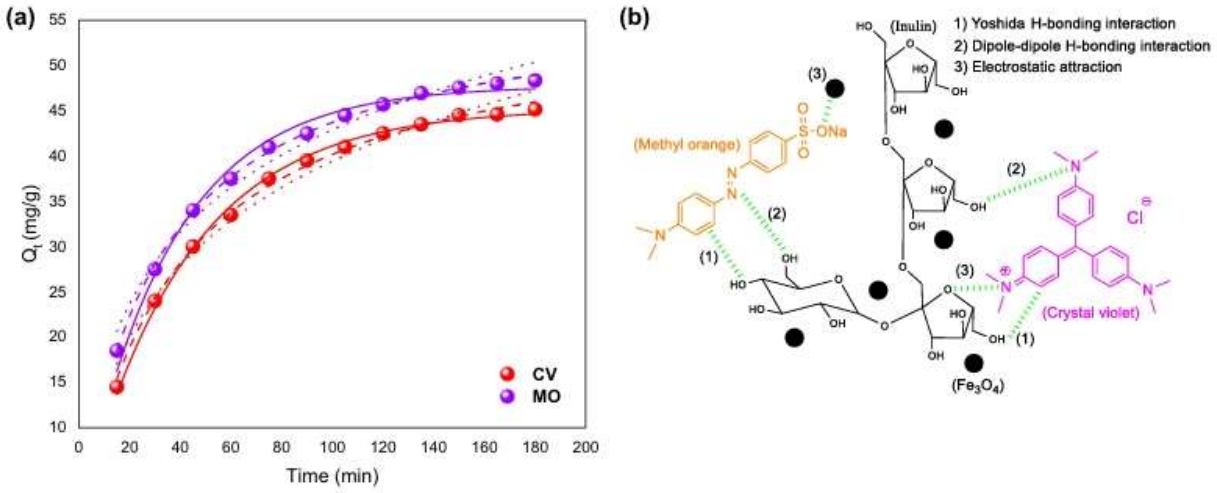

Figure 6. (a) Kinetics data of MO and CV adsorption process at their optimum solution pH predicted by non linear kinetics models at Ca = 0.5 g/L and Cdye = 25 mg/L: solid line: PFO, dashed line: PSO, dotted line: Elovich; (b) proposed mechanism of dye adsorption onto the Fe3O4@inulin nanocomposite.

Parameter	Dye	
	MO	CV
PFO		
Q_e	47.736	45.243
k_1 [min^{-1}]	0.0276	0.0239
Reduced chi-squared	1.148	0.3634
R^2	0.9880	0.9964
Adjusted R^2	0.9868	0.9960
PSO		
Q_e	57.523	56.094
k_2 [g mg^{-1} min^{-1}]	5.501	4.497
Reduced chi-squared	0.1265	0.3192
R^2	0.9986	0.9968
Adjusted R^2	0.9985	0.9965
Elovich		
α [mg/g min]	3.344	2.233
β	0.0764	0.0719
Reduced chi-squared	1.7776	2.0849
R^2	0.9814	0.9793
Adjusted R^2	0.9796	0.9773

Table 2. Fitting parameters obtained from kinetics models for MO and CV adsorption onto the Fe_3O_4@inulin nanocomposite.

$$\Delta G^\circ = -RT \ln K_c \tag{11}$$

$$\ln K_c = -\frac{\Delta H^\circ}{RT} + \frac{\Delta S^\circ}{R} \tag{12}$$

where the adsorption equilibrium constant is Kc. Table 3 shows the thermodynamic data that was calculated from the above equations. Volgens die positive H°-waarde was die adsorption proses endothermic, wat ooreenstem met die feit dat dye adsorption toeneem met temperatuur. Die G-waarde wat negatief is, dui op 'n onafhanklike adsorptionsproses. Daar word getoon dat die G° afneem soos die temperatuur styg, wat beteken dat die adsorption proses beter werk by hoër temperature. Daarbenewens, as gevolg van 'n aantal struktuurveranderinge wat tydens die proses plaasgevind het, het die ΔS° met positiewe hoeveelheid verbeterde randomness by die solution-solid interface getoon. Layers of hydration surrounded the composites and dye molecules in the aqueous solution.

Dye\parameter	ΔH° [kJ/mol] at 298 K	ΔS° [kJ/mol K] at 298 K	ΔG° [kJ/mol]			
			283 K	298 K	313 K	338 K
MO	11.5448	46.0172	−1.4519	−2.1345	−2.9897	−3.9379
CV	10.2271	37.8977	−0.4691	−1.0695	−1.7101	−2.5345

Table 3. Thermodynamic parameters for CO_2 adsorption onto Fe_3O_4@inulin nanocomposite.

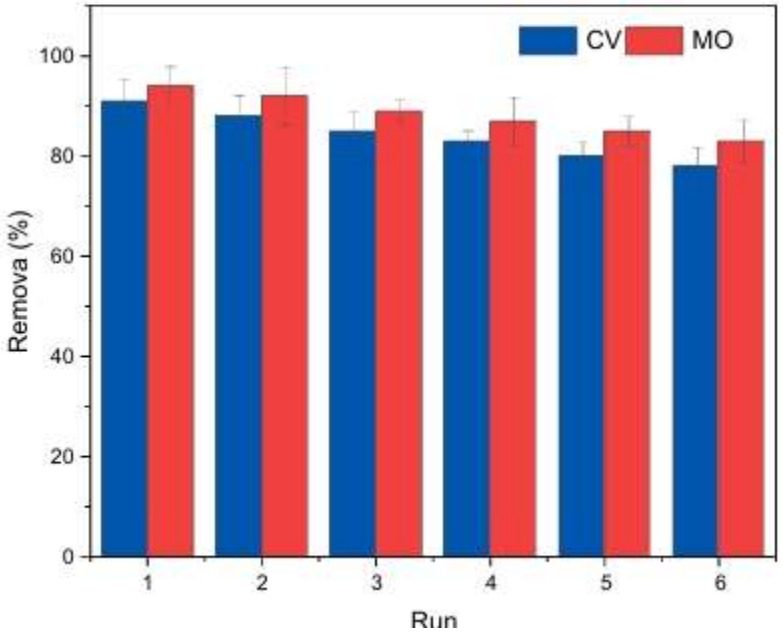

Figure 7. Adsorbent reusability for MO and CV adsorption by Fe3O4@inulin in terms of removal efficiency; T = 298 K, pH = 7 for CV and 5 for MO, Ca = 0.5 g/L, Cdye = 25 mg/L, t = 180 min.

molecules van water. Water molecules ordered in these hydration layers were disturbed and compelled during the adsorption process. This increases the degree of freedom in the adsorbent-dye interaction.

Adsorbent reusability.

Convenient reusability and multi-cycle utilization, asook acceptable adsorption performance, is noodsaaklike elemente vir die skepping van 'n haalbare, scalable, en doeltreffende treatment system. Hierdie elemente beïnvloed adsorbent prestasie en verlaag operationele koste. In order to renew the adsorbent, ethanol and acetone with high dipole moments were utilized as desorption agents. Dye particles adsorbed first onto the Fe3O4@inulin. After adsorption, the adsorbent's dye-containing particles were renewed by ethanol or acetone, washed thoroughly with

DI water, and then used again for dye adsorption.. Six times, the Fe3O4@ inulin was used to verify its suitability for removal of CV and MO dyes. Fig. 7 toon the reusability of both dyes' adsorption under their optimal solution pH and adsorbent dosage. As 'n besonderheid, die removal efficiency van Fe3O4@inulin magnetic composite decreased for MO dyes after six consecutive adsorption cycles, from 94.92 to 83.34% and from 91.13 to 78.86%, respectively. Terselfdertyd het CV dyes voortgegaan om meer as 87% van hul aanvanklike adsorption rates te handhaaf. As sorption sites oorvol is met strongly adsorbed dye molecules, kan adsorption prestasie afneem met 'n groter cycle aantal. As gevolg van sy uitstekende reusbaarheid, toon Fe3O4@inulin hoë MO- en CV-vrystellings... Selfs al het elke sorbent sy eie unieke eienskappe, intrinsieke eienskappe, voordele en nadele, Die Fe3O4@inulin adsorption capacity for MO and CV removal is assesseer in vergelyking met ander bio-nano adsorbents. Tabel 4 vergelyk verskillende bio-adsorbente met betrekking tot hul optimale solusie pH. Daarbenewens word die beste solution pH-, isotherm- en kinetics-modelle opgesom. As getoon, magnetized inulin het 'n groter kapasiteit om beide dyes te verwyder as soortgelyke magnetized biomaterials. Daar word bewys deur hierdie prestasie dat Fe3O4@inulin is 'n uitstekende magnetiese sorbent met goeie stabiliteit wat beide anionic en cationic dyes kan adsorbeer onder die toepaslike pH van die solution.

Conclusion

As gevolg van die toenemende industrialisering regoor die wêreld, is dye-contaminated water nou 'n ernstige kwessie vir die omgewing. As gevolg hiervan moet environmentalists en researchers onmiddellik aandag gee aan die ontwikkeling van doeltreffende metodes en materiale om hierdie kwessies te verlig. We het in hierdie studie 'n nuwe bio-nano adsorbent geskep, magnetized inulin met Fe3O4, om skadelike anionic en cationic dyes uit wastewater te verwyder. The fabrication of the magnetic nanocomposite was assessed through a number of physical and structural analyses. As gevolg van the FTIR spectra, the presence of the Fe–O bond confirmed the successful synthesis of Fe3O4@inulin. According to its XRD pattern, the average crys talline size is 10.9 nm. The SEM–EDX results showed a relatively consistent,

Adsorbent	Dye	Solution pH	Isotherm model	Kinetics model	Q_m [mg/g]	Reusability (cycle and reduction in removal efficiency)	References
Chitosan microspheres	MO	3.1	Langmuir	PSO	207	5 and ~ 9%	45
Modified gum Tragacanth/graphene oxide	CV	8	Langmuir	PSO	94.0	3 and ~ 15%	46
Magnetic lignin-based carbon nanoparticles	MO	5	Langmuir	PSO	113.0	4 & 10%	47
Magnetic starch-graft-poly(acrylic acid) hydrogels	CV	7	Langmuir	PSO	80.64	5 and ~ 5%	48
Layered double hydroxides@Fe_3O_4/PVA	MO	6	Freundlich	PSO	19.59	4 and 50%	49
Magnetic kappa-carrageenan nanocomposite beads	CV	8	Langmuir	PSO	84.7		50
Xanthan gum/PVI hydrogel	CV	7	Langmuir	PFO	453.0		51
Ferric oxide-biochar nanocomposites	MO	8	Freundlich	PSO	20.53		52
Modified cellulose with glycidyl methacrylate	CV	9	Langmuir	PSO	218.8	8 and ~ 30	53
Chitosan/organic rectorite composite	MO	3	Langmuir	PSO	5.56		54
Hydroxyapatite nanoparticles impregnated magnetic bentonite	CV	8	Freundlich	PSO	1290.30	5 and ~ 5%	55
Fe_3O_4@inulin	MO	5	Langmuir	PSO	276.26	6 and ~ 11%	This work
	CV	7	Langmuir	PSO	223.57	6 and ~ 12%	

Table 4. Performance comparison of different bio-nano adsorbents for treating water contaminated with MO and CV dyes. PVA: ed poly (vinyl alcohol), PVI: poly (N-vinyl imidazole)

regular dispersion of spherical nanoparticles with a diameter of 10–20 nm on the surface of the composite. Volgens BET-analise was die adsorbent se specific surface area, pore volume, en gemiddelde pore diameter 66.15 m2/g, 0.181 cm3/g, en 11.027 nm, respectively. As gevolg van die VSM-analise het die nanocomposite se magnetic saturation, wat 40.21 emu/g was, ongeveer 34% laer as dié van pure Fe3O4 nanoparticles. As gevolg van die pHPZC-waarde van 6, asook die anionic en cationic eienskappe van die twee dyes, was die optimale solution pH vir MO 5 en vir CV 7. The Langmuir isotherm fitted better the experimental data with a maximum adsorption capacity, according to the highest R2 value (> 0.99) and the lowest reduced chi-squared. of 276.26 mg/g vir MO en 223.57 mg/g vir CV by 338 K, respectively. In die prediction of the kinetics data of both dyes, the pseudo-second-order model (R2 < 0.99 and reduced chi-squared < 1) outperformed the pseudo-second-order and Elovich models based on these statistical criteria. Furthermore, the thermodynamic parameter showed that the dye adsorption by Fe3O4@inulin was spontaneous and endothermic. Daarbenewens, selfs nadat die adsorbent ses keer gebruik is, het die prepared nanocomposite 'n uitstekende reusbaarheid en stabiliteit getoon, aangesien dit 'n removalskoers van meer as 87% vir beide pollutants behou het. Overall, a comparison of different magnetized adsorbents' ability to adsorb cationic and anionic dyes confirmed that the Fe3O4@inulin could be

References

1. Liang, L. et al. Review of organic and inorganic pollutants removal by biochar and biochar-based composites. Biochar 3, 255–281

(2021).

2. Behroozi, A. H. & Ataabadi, M. R. Improvement in microfiltration process of oily wastewater: A comprehensive review over two

decades. J. Environ. Chem. Eng. 9, 104981 (2021).

3. Khajavian, M., Salehi, E. & Vatanpour, V. Chitosan/polyvinyl alcohol thin membrane adsorbents modified with zeolitic imidazolate

framework (ZIF-8) nanostructures: Batch adsorption and optimization. Sep. Purif. Technol. 241, 116759 (2020).

4. Piri, F., Mollahosseini, A. & Hosseini, M. M. Enhanced adsorption of dyes on microwave-assisted synthesized magnetic zeolite

hydroxyapatite nanocomposite. J. Environ. Chem. Eng. 7, 103338 (2019).

5. Al-Ansari, M. M., Li, Z., Masood, A. & Rajaselvam, J. Decolourization of azo dye using a batch bioreactor by an indigenous bac

terium Enterobacter aerogenes ES014 from the waste water dye effluent and toxicity analysis. Environ. Res. 205, 112189 (2022).

6. Ahmed, D. N., Naji, L. A., Faisal, A. A., Al-Ansari, N. & Naushad, M. Waste foundry sand/MgFe-layered double hydroxides com

posite material for efficient removal of Congo red dye from aqueous solution. Sci. Rep. 10, 1–12 (2020).

7. Koohi, P., Rahbar-kelishami, A. & Shayesteh, H. Efficient removal of congo red dye using Fe3O4/NiO nanocomposite: Synthesis

and characterization. Environ. Technol. Innov. 23, 101559 (2021).

8. Peter, C. et al. N-doped ZnO/graphene oxide: A photostable photocatalyst for improved mineralization and photodegradation of

organic dye under visible light. Ionics 25, 327–339 (2019).

9. Maleki, A. et al. Investigation of potato peel-based bio-sorbent efficiency in reactive dye removal: Artificial neural network mod

eling and genetic algorithms optimization. J. Adv. Environ. Health Res. 1, 21–28 (2013).

10. Moradihamedani, P. Recent advances in dye removal from wastewater by membrane technology: A review. Polym. Bull. 79,

2603–2631 (2021).

11. Ghanbari, F. & Moradi, M. A comparative study of electrocoagulation, electrochemical Fenton, electro-Fenton and peroxi-coagu

lation for decolorization of real textile wastewater: Electrical energy consumption and biodegradability improvement. J. Environ.

Chem. Eng. 3, 499–506 (2015).

12. Xu, S. et al. Influence of output current on decolorization efficiency of azo dye wastewater by a series system with multi-stage

reverse electrodialysis reactors. Energy Convers. Manag. 228, 113639 (2021).

13. Basith, M., Ahsan, R., Zarin, I. & Jalil, M. Enhanced photocatalytic dye degradation and hydrogen production ability of Bi25FeO40

rGO nanocomposite and mechanism insight. Sci. Rep. 8, 1–11 (2018).

14. Nguyen, D. L. T. et al. Metal salt-modified biochars derived from agro-waste for effective congo red dye removal. Environ. Res.

200, 111492 (2021).

15. Rodrigues, C. S., Madeira, L. M. & Boaventura, R. A. Synthetic textile dyeing wastewater treatment by integration of advanced

oxidation and biological processes—Performance analysis with costs reduction. J. Environ. Chem. Eng. 2, 1027–1039 (2014).

16. Wong, S. et al. Effective removal of anionic textile dyes using adsorbent synthesized from coffee waste. Sci. Rep. 10, 1–13 (2020).

17. Bayomie, O. S. et al. Novel approach for effective removal of methylene blue dye from water using fava bean peel waste. Sci. Rep.

10, 1–10 (2020).

18. Ali, F., Khan, S. B., Kamal, T., Alamry, K. A. & Asiri, A. M. Chitosan-titanium oxide fibers supported zero-valent nanoparticles:

Highly efficient and easily retrievable catalyst for the removal of organic pollutants. Sci. Rep. 8, 1–18 (2018).

19. Jawad, A. H., Mubarak, N. S. A. & Abdulhameed, A. S. Hybrid crosslinked chitosan-epichlorohydrin/TiO2 nanocomposite for

reactive red 120 dye adsorption: Kinetic, isotherm, thermodynamic, and mechanism study. J. Polym. Environ. 28, 624–637 (2020).

20. Reghioua, A. et al. Magnetic chitosan-glutaraldehyde/zinc oxide/Fe3O4 nanocomposite: Optimization and adsorptive mechanism

of remazol brilliant blue R dye removal. J. Polym. Environ. 29, 3932–3947 (2021).

21. Kazemi, J. & Javanbakht, V. Alginate beads impregnated with magnetic Chitosan@ Zeolite nanocomposite for cationic methylene

blue dye removal from aqueous solution. Int. J. Biol. Macromol. 154, 1426–1437 (2020).

22. Al-Musawi, T. J., Mengelizadeh, N., Al Rawi, O. & Balarak, D. Capacity and modeling of acid blue 113 dye adsorption onto chitosan

magnetized by Fe2O3 nanoparticles. J. Polym. Environ. 30, 344–359 (2022).

23. Tanhaei, B., Ayati, A., Iakovleva, E. & Sillanpää, M. Efficient carbon interlayed magnetic chitosan adsorbent for anionic dye removal:

Synthesis, characterization and adsorption study. Int. J. Biol. Macromol. 164, 3621–3631 (2020).

24. de Figueiredo Neves, T. et al. Novel magnetic chitosan/quaternary ammonium salt graphene oxide composite applied to dye

removal. J. Environ. Chem. Eng. 8, 103820 (2020).

25. Hernández-Martínez, A. R. et al. Evaluation of inulin replacing chitosan in a polyurethane/polysaccharide material for Pb2+

removal. Molecules 22, 2093 (2017).

26. Qi, X. et al. Recent advances in polysaccharide-based adsorbents for wastewater treatment. J. Clean. Prod. 315, 128221 (2021).

27. Gaio, I. et al. Liquefied petroleum gas as solvent medium for the treatment of immobilized pectinases. Biocatal. Agric. Biotechnol.

11, 108–115 (2017).

28. Sirajudheen, P., Nikitha, M. R., Karthikeyan, P. & Meenakshi, S. Perceptive removal of toxic azo dyes from water using magnetic

Fe3O4 reinforced graphene oxide–carboxymethyl cellulose recyclable composite: Adsorption investigation of parametric studies

and their mechanisms. Surf. Interfaces 21, 100648 (2020).

29. Bateni, A., Valizadeh, K., Salahshour, Y., Behroozi, A. H. & Maleki, A. Fabrication and characterization of pectin-graphene oxide

magnesium ferrite-zinc oxide nanocomposite for photocatalytic degradation of diclofenac in an aqueous solution under visible

light irradiation. J. Environ. Manag. 324, 116358 (2022).

30. Fashi, F., Ghaemi, A. & Behroozi, A. H. Piperazine impregnation on Zeolite 13X as a novel adsorbent for CO2 capture: Experimental

and modeling. Chem. Eng. Commun. 208, 1104–1120 (2021).

31. Vatanpour, V. et al. Investigation of boron nitride/silver/graphene oxide nanocomposite on separation and antibacterial improve

ment of polyethersulfone membranes in wastewater treatment. J. Environ. Chem. Eng. 10, 107035 (2022).

32. Maleki, A., Hassanzadeh-Afruzi, F., Varzi, Z. & Esmaeili, M. S. Magnetic dextrin nanobiomaterial: an organic-inorganic hybrid

catalyst for the synthesis of biologically active polyhydroquinoline derivatives by asymmetric Hantzsch reaction. Mater. Sci. Eng.,

C 109, 110502 (2020).

33. Rani, N. et al. X-ray analysis of MgO nanoparticles by modified Scherer's Williamson-Hall and size-strain method. Mater. Today

Proc. 12, 543–548 (2019).

34. Rahman, M. M., Muttakin, M., Pal, A., Shafiullah, A. Z. & Saha, B. B. A statistical approach to determine optimal models for

IUPAC-classified adsorption isotherms. Energies 12, 4565 (2019).

35. Kayan, A. Inorganic-organic hybrid materials and their adsorbent properties. Adv. Compos. Hybrid Mater. 2, 34–45 (2019).

36. El Naga, A. O. A., Shaban, S. A. & El Kady, F. Y. Metal organic framework-derived nitrogen-doped nanoporous carbon as an

efficient adsorbent for methyl orange removal from aqueous solution. J. Taiwan Inst. Chem. Eng. 93, 363–373 (2018).

37. Purkait, M. K., Maiti, A., DasGupta, S. & De, S. Removal of congo red using activated carbon and its regeneration. J. Hazard. Mater.

145, 287–295. https://doi.org/10.1016/j.jhazmat.2006.11.021 (2007).

38. Kamran, U., Bhatti, H. N., Noreen, S., Tahir, M. A. & Park, S.-J. Chemically modified sugarcane bagasse-based biocomposites for

efficient removal of acid red 1 dye: Kinetics, isotherms, thermodynamics, and desorption studies. Chemosphere 291, 132796 (2022).

39. Ghaemi, A. & Behroozi, A. H. Comparison of hydroxide-based adsorbents of Mg(OH)2 and Ca(OH)2 for CO2 capture: Utilization

of response surface methodology, kinetic, and isotherm modeling. Greenhouse Gases Sci. Technol. 10, 948–964 (2020).

40. Maryanti, R., Nandiyanto, A. B. D., Manullang, T. I. B., Hufad, A. & Sunardi, S. Adsorption of dye on carbon microparticles:

Physicochemical properties during adsorption, adsorption isotherm and education for students with special needs. Sains Malays.

49, 2949–2960 (2020).

41. Jain, N. & Maiti, A. Fe–Mn–Al metal oxides/oxyhydroxides as As(III) oxidant under visible light and adsorption of total arsenic

in the groundwater environment. Sep. Purif. Technol. 302, 122170 (2022).

42. Nakarmi, K. J. et al. Synthesis of biochar from iron-free and iron-containing microalgal biomass for the removal of pharmaceuticals

from water. Environ. Res. 214, 114041. https://doi.org/10.1016/j.envres.2022.114041 (2022).

43. Mittal, H., Al Alili, A., Morajkar, P. P. & Alhassan, S. M. Graphene oxide crosslinked hydrogel nanocomposites of xanthan gum

for the adsorption of crystal violet dye. J. Mol. Liq. 323, 115034 (2021).

44. George, G. & Saravanakumar, M. P. Facile synthesis of carbon-coated layered double hydroxide and its comparative characterisa

tion with Zn–Al LDH: application on crystal violet and malachite green dye adsorption—Isotherm, kinetics and Box-Behnken

design. Environ. Sci. Pollut. Res. 25, 30236–30254 (2018).

45. Zhai, L., Bai, Z., Zhu, Y., Wang, B. & Luo, W. Fabrication of chitosan microspheres for efficient adsorption of methyl orange. Chin.

J. Chem. Eng. 26, 657–666 (2018).

46. Sahraei, R., Pour, Z. S. & Ghaemy, M. Novel magnetic bio-sorbent hydrogel beads based on modified gum tragacanth/graphene

oxide: Removal of heavy metals and dyes from water. J. Clean. Prod. 142, 2973–2984 (2017).

47. Ma, Y.-Z., Zheng, D.-F., Mo, Z.-Y., Dong, R.-J. & Qiu, X.-Q. Magnetic lignin-based carbon nanoparticles and the adsorption for

removal of methyl orange. Colloids Surf., A 559, 226–234 (2018).

48. Pourjavadi, A., Hosseini, S. H., Seidi, F. & Soleyman, R. Magnetic removal of crystal violet from aqueous solutions using polysac

charide-based magnetic nanocomposite hydrogels. Polym. Int. 62, 1038–1044 (2013).

49. Mallakpour, S. & Hatami, M. An effective, low-cost and recyclable bio-adsorbent having amino acid intercalated LDH@ Fe3O4/

PVA magnetic nanocomposites for removal of methyl orange from aqueous solution. Appl. Clay Sci. 174, 127–137 (2019).

50. Mahdavinia, G. R., Iravani, S., Zoroufi, S. & Hosseinzadeh, H. Magnetic and K+-cross-linked kappa-carrageenan nanocomposite

beads and adsorption of crystal violet. Iran. Polym. J. 23, 335–344 (2014).

51. Mohamed, R. R., Abu Elella, M. H., Sabaa, M. W. & Saad, G. R. Synthesis of an efficient adsorbent hydrogel based on biodegradable

polymers for removing crystal violet dye from aqueous solution. Cellulose 25, 6513–6529 (2018).

52. Chaukura, N., Murimba, E. C. & Gwenzi, W. Synthesis, characterisation and methyl orange adsorption capacity of ferric oxide—

Biochar nano-composites derived from pulp and paper sludge. Appl. Water Sci. 7, 2175–2186 (2017).

53. Zhou, Y. et al. Removal of crystal violet by a novel cellulose-based adsorbent: Comparison with native cellulose. Ind. Eng. Chem.

Res. 53, 5498–5506 (2014).

54. Zeng, L. et al. Chitosan/organic rectorite composite for the magnetic uptake of methylene blue and methyl orange. Carbohydr.

Polym. 123, 89–98 (2015).

55. Ain, Q. U. et al. Facile fabrication of hydroxyapatite-magnetite-bentonite composite for efficient adsorption of Pb(II), Cd(II), and

crystal violet from aqueous solution. J. Clean. Prod. 247, 119088 (2020).